

Identifying High Accuracy Regions in Traffic Camera Images to Enhance the Estimation of Road Traffic Metrics: A Quadtree Based Method

Yue Lin^{a*}, Ningchuan Xiao^{a,b}

^a *Department of Geography, The Ohio State University, Columbus, Ohio*

^b *Center for Urban and Regional Analysis, The Ohio State University, Columbus, Ohio*

*Corresponding author: lin.3326@osu.edu

Abstract: The growing number of real-time camera feeds in urban areas has made it possible to provide high-quality traffic data for effective transportation planning, operations, and management. However, deriving reliable traffic metrics from these camera feeds has been a challenge due to the limitations of current vehicle detection techniques, as well as the various camera conditions such as height and resolution. In this work, a quadtree based algorithm is developed to continuously partition the image extent until only regions with high detection accuracy are remained. These regions are referred to as the high-accuracy identification regions (HAIR) in this paper. We demonstrate how the use of the HAIR can improve the accuracy of traffic density estimates using images from traffic cameras at different heights and resolutions in Central Ohio. Our experiments show that the proposed algorithm can be used to derive robust HAIR where vehicle detection accuracy is 41 percent higher than that in the original image extent. The use of the HAIR also significantly improves the traffic density estimation with an overall decrease of 49 percent in root mean squared error.

Keywords: traffic count; traffic density estimation; object detection; deep learning; region quadtree; image segmentation

1 Introduction

The past two decades have witnessed a surge in world vehicle ownership (Davis and Boundy, 2020) that not only aggravates many negative externalities of the transportation systems such as road congestion and air pollution in urban areas, but also threatens the sustainability of the human-environment systems worldwide (Essen et al., 2019). To address these issues, many countries have started to adopt effective approaches to transportation operations, all of which require accurate and real-time road traffic metrics such as traffic density, flow, and speed. In transport and urban planning, road traffic metrics offer critical data support to the arrangement of transport services and infrastructure that facilitates equitable access to employment, system reliability, and social/environmental justice (Black, 2018). Today, road traffic metrics are widely applied in various areas, including routing (Kim et al., 2005), dynamic congestion pricing (de Palma and Lindsey, 2011; Olszewski and Xie, 2005), traffic emission control (Sookun et al., 2014; Xu et al., 2018), and intelligent transportation systems (Smith, 2017).

Since the early 2000s, traffic cameras have rapidly emerged as a primary data source in the field of transportation, particularly in the United States and Canada. Real-time images from these cameras are typically available to the public. The April release of the Traffic Video Mobile App by TrafficLand (2020), for example, provides access to more than 25,000 traffic cameras in over 200 cities in the United States for the public to use through free subscriptions. These publicly available camera feeds have the potential of being used to provide accurate and real-time road traffic metrics at scale with relatively low additional capital costs. Many vehicle detection methods have been developed to process these camera images for road traffic metric estimation, and significant progress has been made in this area since several deep learning approaches are proposed (see a review in the next section). However, vehicles on the same images are not equally detectable. As indicated by Zhang et al. (2016), objects in the foreground of an image can generally be detected with high accuracy by most object detection methods, while those in the

parts of view distant from the camera due to tilt and perspective are often too small to be detected. Missed and/or falsely identified small vehicles tend to result in significant errors in the estimation of road traffic metrics.

The purpose of this paper is to develop an effective method that can be used to obtain accurate traffic estimates from camera feeds. We focus on identifying the subset of pixels in each image where vehicles can be correctly detected, which, in turn, can be used to derive reliable and accurate road traffic metrics such as traffic density. More specifically, we develop a quadtree based algorithm to systematically partition the image in a recursive manner so that only the high accuracy regions in the image will be maintained. These regions are referred to as the high-accuracy identification regions (HAIR). In the remainder of this paper, Section 2 discusses the rationale of this research by examining the limitations of existing data sources and vehicle detection methods. Section 3 presents our algorithm for HAIR identification that helps improve the accuracy of the road traffic metrics derived from camera images. In Section 4, the proposed algorithm is applied to the traffic camera data collected in Central Ohio for accurate traffic density estimation. The paper is concluded in Section 5.

2 Background and Rationale

Road traffic metrics can be obtained from different data sources. For example, vehicular networks formed by vehicle-to-vehicle (V2V) communication technology have been used to provide road traffic metrics (Shin et al., 2020; Wang et al., 2018). This approach relies on participating private or commercial vehicles with built-in global positioning system (GPS) trackers, while recruiting participants can be time-consuming and costly. Other methods use data from mobile phone tracking, which are often restricted by the device usages and may be subject to privacy concerns regarding the identities and private movement behaviors of users (Huang et al., 2020). Data sets developed based on V2V or mobile phone tracking are generally not accessible to the public, which also limits their applications in transportation. Another type of method utilizes traffic sensors including loop detectors, pneumatic tubes, and light detection and ranging (LiDAR) sensors (Zhang et al., 2019; Zhao et al., 2019). However, these sensors often suffer from relatively short lifetimes, high capital costs in maintenance, and limited spatial coverage, and therefore have not been prevalently adopted for robust traffic monitoring (Leduc, 2008).

Traffic camera feeds are an emerging data source that is publicly accessible and has a wide coverage. Vehicle detection is an essential step to extract road traffic information from the camera feeds. Traditional vehicle detection methods utilize classical computer vision techniques such as edge and corner detection to identify the presence of individual vehicles from images (Chung and Sohn, 2018; Snyder and Do, 2019). However, these methods are based on low-level vehicle features (e.g., straight lines and dots on the vehicle) that are small and simple, which often leads to a considerable number of missing and falsely detected vehicles in the images (O’Mahony et al., 2020). Over the past decade, the rapid development of deep learning methods, especially the recent breakthrough of convolutional neural networks (CNN), has significantly improved the accuracy of many computer vision applications including vehicle identification (Cao et al., 2016; Chung and Sohn, 2018). CNN is a class of deep neural networks that is able to automatically detect and “learn” high-level features representing larger and more complex vehicle elements (e.g., wheels of a vehicle), which, compared to traditional computer vision methods, can utilize more informative and representative features to detect vehicles in the images (O’Mahony et al., 2020). To date, a set of CNN-based object detectors have been developed and applied to vehicle detection, including Faster R-CNN (Ren et al., 2017), YOLO v4 (Wang and Liao, 2020), RetinaNet (Lin et al., 2020), and EfficientDet (Tan et al., 2020).

Existing deep learning detectors heavily depend on the level of detail of the vehicles present in the images to make accurate detections. As indicated by Wang et al. (2019), for vehicles with ground truth bounding box sizes larger than 40 pixels, the average precision in detection can generally reach above 0.8, because details of the vehicle element and feature are clearly displayed in the images. When the vehicle sizes are below 25 pixels, the average precision drops to approximately 0.4, implying that a large number of vehicles are missed and/or falsely identified. Figure 1 presents two examples of using a deep learning detector to identify the vehicles in traffic images (see the Appendix for details about the detector). Due to the tilts and perspectives of traffic cameras, the level of detail of the on-road vehicles can vary significantly on the same image. Vehicles distant from the cameras can be in small sizes and even not identifiable with the naked eye. These distant and small vehicles in the image lack detailed vehicle features and therefore are unlikely to be correctly identified by vehicle detectors (Fattal et al., 2018; Huang et al., 2017).



Figure 1. Two examples of using EfficientDet (Tan et al., 2020) to identify vehicles in traffic images. Rectangles with blue outlines are the ground truth bounding boxes of missed vehicles, and those with green outlines are the bounding boxes of vehicles predicted by the model.

The tendency of vehicle detectors in misclassifying distance vehicles in the image leads to a dilemma when we use the detected vehicles to compute road traffic metrics: should we use the entire image or just the part where detected vehicles are presented in the image? For example, calculating traffic density in an area relies on the accurate measures of both vehicle count and road length. It is inappropriate to use the entire image as the area because the vehicles in the distant areas from the camera are almost certain not to be “counted” by the vehicle detector used (note that all vehicle detection methods have similar performance over these vehicles), and subsequently dividing the vehicle count by the road length in the entire image extent is erroneous. Fortunately, this threat to internal validity (McDermott, 2011) can be effectively addressed by simply excluding the areas where errors tend to occur. In other words, we establish a region formed by a subset of the pixels in the image where we can consistently detect vehicles accurately. We call these regions the high accuracy identification regions, or HAIR. Vehicles appearing outside the HAIR, detected or not, will not be counted. In the same fashion, only roads within the HAIR will be used for traffic density (or other metric, such as speed) calculation.

3 Methodology

Three important factors need to be considered when constructing the HAIR: accuracy, consistency, and efficiency. First, a high and desired vehicle detection accuracy, as specified by the user, should be reached within the HAIR. While there may not exist an objective accuracy level, users on

different applications often have their desirable accuracy, and the algorithm should be able to identify regions that exceeds such an accuracy threshold. Second, we should expect the HAIR to perform consistently for new (existing or future) images with the same field of view. And finally, the calculation of HAIR should be efficient as it should not add computational burden to the vehicle detection process.

These three requirements help us explore the use of image segmentation algorithms in the field of computer vision for HAIR identification. Image segmentation refers to the process of continuously partitioning an image into regions until the regions become homogeneous (R. Pal and K. Pal, 1993), and a particular image segmentation process that uses a region quadtree (Samet, 1984; Spann and Wilson, 1985; Xiao, 2016) to guide the partitioning process has proven to be efficient and consistent (Conde Márquez et al., 2011; Spann and Wilson, 1985). In this algorithm, an image is divided into four equal quadrants, and if a quadrant is not homogeneous, it will be further decomposed into smaller quadrants. Figure 2 illustrates such a process. A parameter called depth is used to describe the level of partitioning, and the example in Figure 2d has a depth of 3. We adopt this approach and develop a similar algorithm that continues to partition a traffic camera image so that the high accuracy regions can be established.

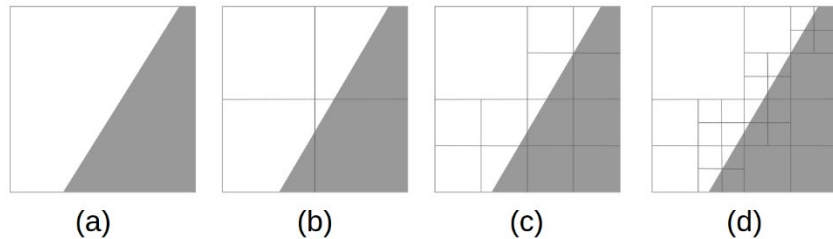


Figure 2. A quadtree based image segmentation process. The heterogeneous image (a) is divided into 4 equal quadrants (b). All quadrants in (b), except for the for the upper-left one, are heterogeneous and need to be further partitioned into smaller quadrants (c). The partitioning process stops at depth 3 (d).

3.1 Quadtree based algorithm for HAIR identification

The purpose of our algorithm is to determine the regions in a camera’s field of view to be the HAIR. This algorithm requires three user inputs. First, a set of images is needed where each image contains (1) the manually labeled vehicle bounding boxes that are confirmed to be the ground truth of the vehicles to be detected, and (2) the bounding box of each detected vehicle yielded by some model. We use N to denote the number of images.

The second parameter relates to the accuracy we aim to achieve by identifying the regions of the image as the HAIR. In our process, the image is partitioned into four equal quadrants and the partitioning of a quadrant stops when the accuracy *within* the quadrant is higher than a user-specified threshold (a_0). To evaluate the vehicle detection accuracy of a given region (a quadrant, the entire image, or any arbitrary region), we first compile the bounding boxes of all the vehicles in the region. We ensure that each vehicle (detected or labeled) belongs to one and only one region. If a vehicle’s bounding box intersects with multiple regions, the vehicle will be assigned to the region with the largest overlapping area. The bounding box of each detected vehicle (B_d) is compared to that of its closest labeled vehicle (B_{gt}) to determine whether the detection is correct. A metric called intersection over union (IoU) is calculated as the ratio between the intersected area of B_d and B_{gt} and their union area:

$$IoU = \frac{area(B_d \cap B_{gt})}{area(B_d \cup B_{gt})} \quad (1)$$

When the IoU value exceeds 0.5 (or 50 percent), more than a half the detected bounding box overlaps with a vehicle that is considered as its ground truth, and it is reasonable to say that this vehicle is correctly detected (Everingham et al., 2010). A correctly detected vehicle is a true positive. A detected vehicle with an IoU value smaller than 0.5 is a false positive because we cannot find a vehicle in the ground truth to match it. Ground truth vehicles that are not detected by the model are the false negatives.

For a given region, we define a metric called the regional average precision (RAP) to evaluate its vehicle detection accuracy. RAP is similar to the average precision in the literature (Everingham et al., 2010). Each detected vehicle is associated with a confidence score reported by the vehicle detector to indicate its predicted probability of being a vehicle object. Based on the confidence scores, the list of the detected vehicles in the region is sorted in a descending order. At each position (i) in the list, we have a pair of values: precision (p_i) and recall (r_i). The recall at position i is calculated as the ratio between the number of true positives from the beginning of the list to i and the number of all ground truth vehicles (i.e., true positives + false negatives) within the region. The precision at position i is the ratio between the number of true positives and the number of the detected vehicles (i.e., true positives + false positives) from the beginning of the list to i . Let $R = \{r_1, r_2, \dots, r_M\}$ be a sequence of M recall levels where $r_1 = 0$, $r_M = 1$, and $r_k \leq r_{k+1}$ ($1 \leq k < M$), and $p_i^{\max} = \max \{p_k, k \geq i\}$ be the maximum precision value at recall level r_i (i.e., the maximum precision associated with recall values exceeding r_i). To define the recall levels, R , a common practice in the literature (Everingham et al., 2010) is to use 11 equally spaced values (i.e., $R = \{0, 0.1, \dots, 1\}$), which is also used in this paper. The RAP metric is the average of the maximum precision values at all recall levels in R :

$$RAP = \frac{1}{M} \sum_i p_i^{\max} \tag{2}$$

Figure 3 presents a hypothetical example of how the RAP of a region can be calculated when we have multiple images from a camera. In this case, the entire image is the region. Within each image, the detected vehicles are classified as either true or false positives, and all missed vehicles (false negatives) are also marked. In this example, the RAP value is 0.55. In a practical sense, a high RAP score indicates a high probability of vehicles in a given region being correctly detected. It can be observed that if the region is partitioned into four quadrants, both the lower-left and lower-right quadrants may have higher RAP values (more on this in the next section).

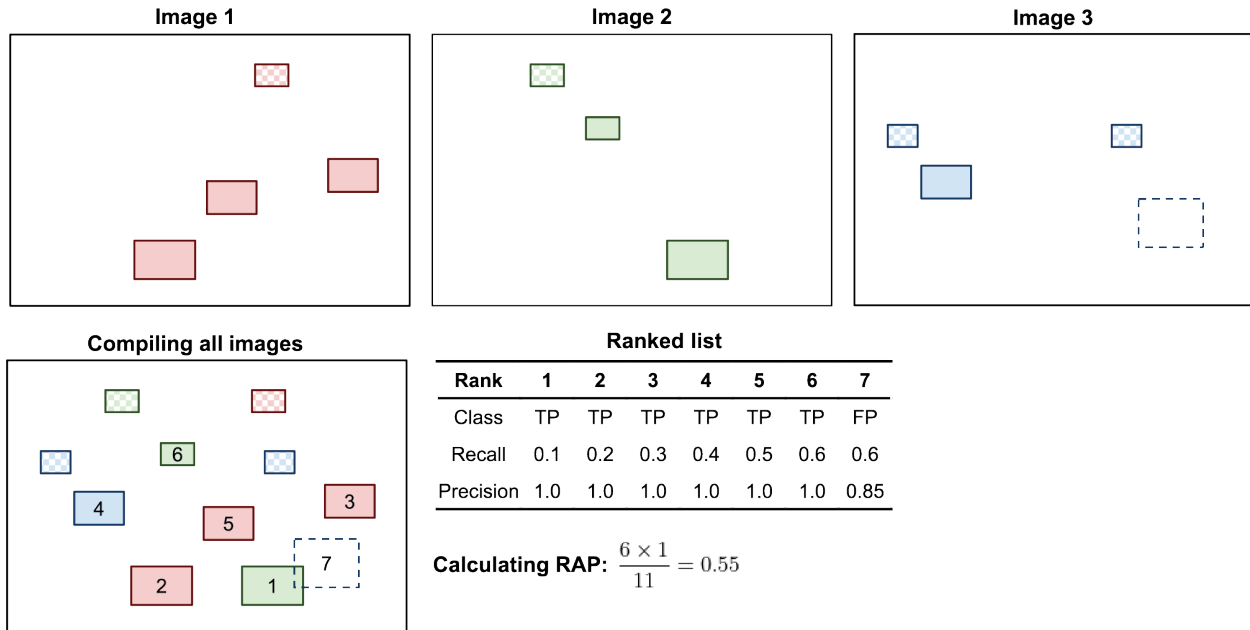


Figure 3. An example of calculating the RAP of a hypothetical region using 3 images from a camera. Rectangles with a solid fill are the bounding boxes of correctly detected vehicles (true positives or TP), and those with a checkerboard fill are the bounding boxes of missed vehicles (false negatives or FN). The rectangle with a dashed outline is a falsely detected vehicle (false positive or FP). Numbers in the compiled region are hypothetical ranks of confidence score for each detected vehicle, reflecting the trend that vehicles close to the camera tend to have high confidence scores. The maximum precision values are 1 at 6 recall levels from 0.1 to 0.6, respectively, while the rest are 0, and therefore the RAP value is 0.55.

The third parameter is the maximal depth (d_0) used in the algorithm to control the level of partitioning. Even though the partitioning continues until the vehicle detection accuracy of a quadrant reaches the accuracy threshold (a_0), theoretically each image can be partitioned to the level of a single pixel, which is unnecessary because vehicle bounding boxes are always larger than that.

These three parameters (number of images, N , accuracy threshold, a_0 , and maximal depth, d_0) are user-specified and will affect the output of the algorithm. We will examine their impact in the next section. The quadtree based HAIR identification algorithm is a recursive algorithm that consists of steps outlined below, where I denotes the region (entire image or a quadrant at any depth) to be examined, H is a list to store the quadrants that form the HAIR, and d is the current depth.

- Step 1.** Set I to the entire image, H to an empty list, and d to 0.
- Step 2.** Combine all the detected and labeled vehicles that fall within I in the N images, and compute the RAP of I using Equation 2. If the RAP is greater than a_0 , add I to H and stop.
- Step 3.** If d equals d_0 , stop.
- Step 4.** Partition the image into 4 equal quadrants and increase d by 1.
- Step 5.** For each quadrant, set I to the quadrant and repeat from Step 2.

Figure 4 illustrates the quadtree based HAIR identification algorithm using one traffic image. For the purpose of demonstration, we set the accuracy threshold (a_0) to 0.75, and the maximal depth (d_0) to 3. Without showing the detailed calculation, we note the RAP value of the original image extent (Figure 4a) is 0.727. This is lower than a_0 and therefore the image will be partitioned into four equal quadrants (Figure 4b). At depth 1, the southwest (lower-left), southeast (lower-right), and northeast (upper-right) quadrants now have an RAP value of 1, and they will be included in the HAIR (rendered in red) and will

not be further partitioned. The other quadrant, however, still has the RAP value lower than 0.75 and the partitioning continues. Figure 4c shows the result of the partitioning at depth 2, where all the four new quadrants are still below the threshold. After the next round of partitioning (depth 3), three additional quadrants at this depth exhibit the RAP higher than the threshold a_0 and are then added into the HAIR, while others still have low RAP values (Figure 4d). Since the current depth is equal to d_0 , the partitioning process stops at this level and the HAIR for this image is finalized. In some cases, further decomposing the image may lead to more regions being included into the HAIR. But it should be noted that such decomposition may become meaningless if the resulting sub-quadrants are too small to contain vehicle bounding boxes. We will examine the impact of the depth in Section 4 where computational experiments are discussed.

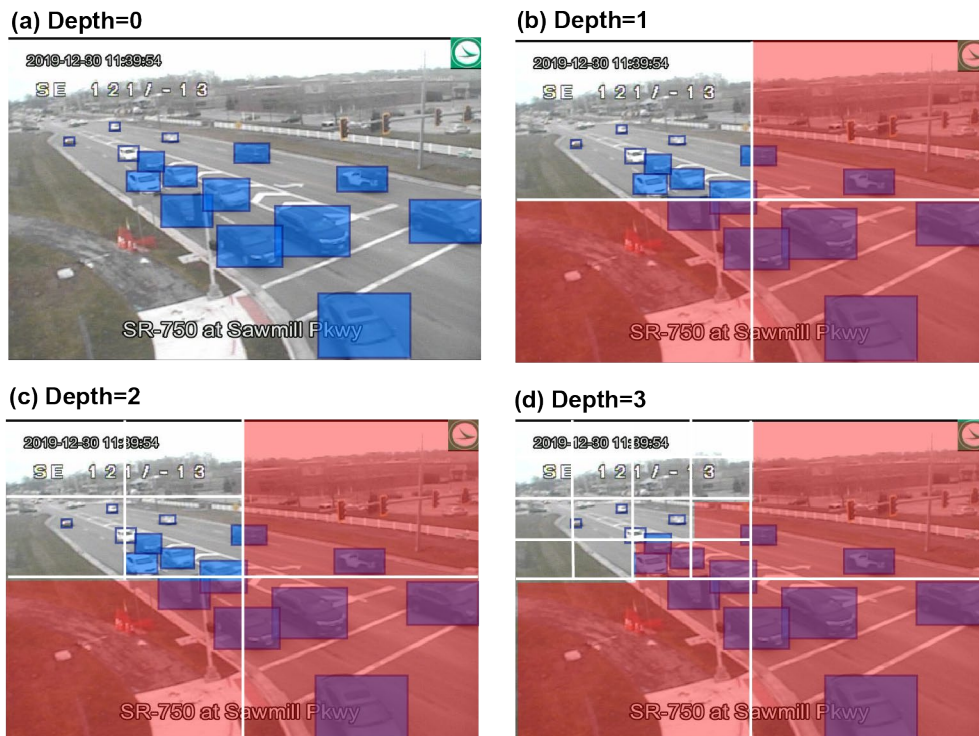


Figure 4. An example of using the quadtree based algorithm for HAIR identification. Regions rendered in red are parts of the HAIR obtained at different depths. Rectangles with blue outlines are the bounding boxes of annotated vehicles, where the filled blue rectangles are vehicles that are correctly detected (true positives), and the open ones are those not detected (false negatives).

3.2 Error measurement

The HAIR is designed to focus on the regions in an image where vehicles are accurately detected. The ultimate error of using the HAIR arises when vehicles that can be accurately detected are not included in the HAIR. Such an error can be introduced in two situations. The first situation occurs when the images used are not representative in covering sufficient on-road vehicle positions. The HAIR derived using insufficient number of images, for example, may cause the error because vehicles on new images may appear at locations that have not been considered in the algorithm. Error may also occur in a situation when a small value of depth is used. For example, in Figure 4, many correctly detected vehicles will be excluded from the HAIR if the process stops at depth 2.

We define the error of the HAIR, e , as the loss of accuracy caused by only including the vehicles in the HAIR. In Figure 5, acc_1 is the RAP value calculated using all the detected vehicles, which is 0.55.

We can then calculate another RAP value, acc_2 , using only the detected vehicles that fall inside the HAIR, and in this case all but the one marked as rank 6 are included. If there are correctly detected vehicles outside the HAIR, acc_2 will be lower than acc_1 . In our example here, the error is 0.1. In an ideal situation, all detected vehicles are in the HAIR, and acc_2 will be as same as acc_1 , meaning the error is zero and the use of the HAIR does not induce error.

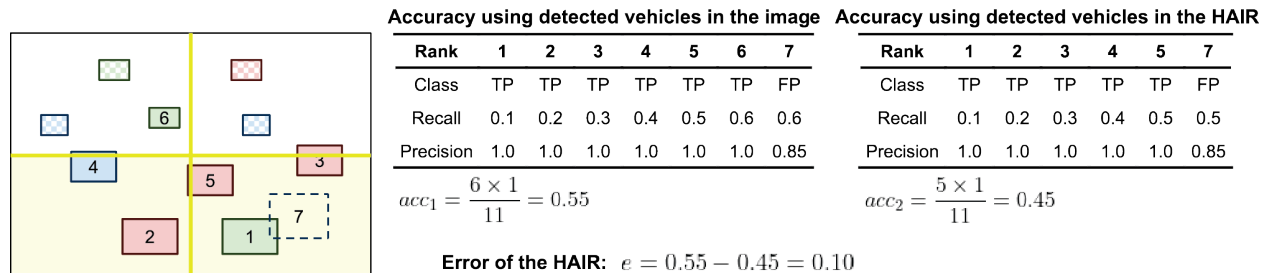


Figure 5. An example of calculating the error brought about by the use of the HAIR. The region here denotes the image extent, and the HAIR includes the two lower quadrants (in yellow). All the correct detections fall in the HAIR except the one ranked 6th.

At this point, one may wonder whether the use of the HAIR can improve the accuracy of vehicle detection. It is important to clarify that the HAIR does not improve vehicle detection accuracy per se. The HAIR is meant to improve the accuracy of estimation of road traffic metrics such as traffic density. The example in Figure 5 demonstrates this point. If we calculate the traffic density by dividing the number of detected vehicles (7) by the total road length within the image, it will clearly underestimate the density because many of the vehicles in the upper part of the image are not counted, and yet the road lengths in that part is used. The estimation can be improved if we only focus on the (lower) part of the image where the vehicles are more correctly detected, and dividing the number of vehicles by the road length in that region (i.e., the HAIR) provides a more truthful estimation. The use of the HAIR allows us to only focus on the areas where vehicles are correctly detected and exclude those areas where we cannot correctly detect them. We will further elaborate on this point in the next section.

4 Computational Experiments and Results

To demonstrate the effectiveness of the HAIR identification algorithm, we apply it to the images from 6 traffic cameras in the metropolitan area around Columbus, Ohio to improve the accuracy of traffic density estimation. These cameras are deployed by the Ohio Department of Transportation (ODOT), with different mounting height and resolutions. Their configuration details, along with an example image from each of them are presented in Figure 6.

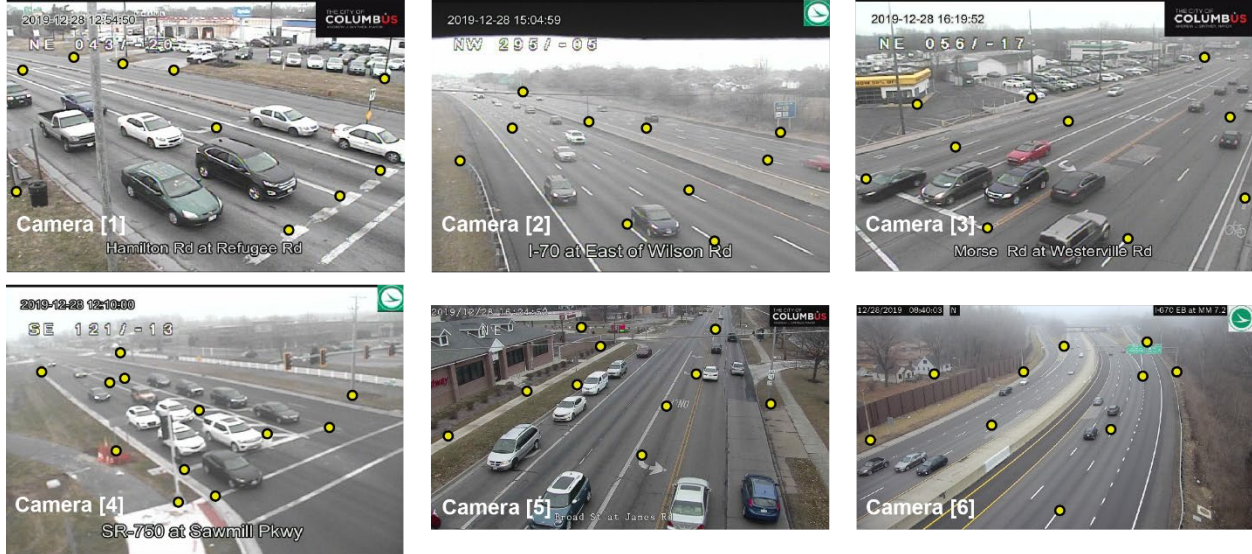


Figure 6. Sample images taken by the 6 selected traffic cameras. Cameras [1], [3], [4], and [5] are mounted low along local roads, each capturing a road section of approximately 420 feet within its field of view. Cameras [2] and [6] are mounted high on highways, and each captures over 0.25 miles of the road sections. In addition, cameras [1], [2], [3], and [4] are low-resolution at 704×480 pixels, while cameras [5] and [6] have a higher resolution of 1920×1080 pixels. Yellow dots on each image are ground control points used for georeferencing (see Section 4.2).

The use of HAIR assumes that some object detector is available to identify the vehicles present in the images, and an image data set can be developed where vehicles are labeled and detected. The algorithm for HAIR identification does not depend on the specific vehicle detector. We train and test a deep learning model called EfficientDet (Tan et al., 2020) to detect the vehicles in the images. Details of the training and testing are discussed in the [Appendix](#). Then, we collect a random sample of 110 images for each camera during the daytime in December 2019, where all the motor vehicles present in the images are manually identified and labeled as the ground truths. The number of images used here (110) is determined based on multiple preliminary trials, and we further discuss the impact of image numbers in Section 4.1. The best detector trained and tested is used to detect the vehicles in the 110 images of each camera. Based on the labeled ground truth and detected vehicles, we conduct two sets of experiments. The first is to identify the HAIR for each camera, and the second to estimate and assess traffic density in the HAIR.

4.1 HAIR identification and assessment

A resampling procedure (James et al., 2013) is adopted to find the parameter values for the quadtree based algorithm so that the average error brought about by the HAIR is minimized for each camera. Here, N images are randomly sampled from the 110 images of each camera. These N images are used to obtain the HAIR for each camera. The value of N is systematically changed from 10 to 100 with an interval of 10, and at each N value, the maximal depth (d_0) is systematically changed from 1 to 5. We adopt an RAP threshold (a_0) of 0.75 that is considered to be a high accuracy in vehicle detection within the given region (Everingham et al., 2010). The error of the HAIR (e , see section 3.2) obtained for each combination of N and d_0 is evaluated using 10 images sampled from the remaining $110 - N$ images. We repeat this process (sampling N images, obtaining the HAIR, computing the error using 10 random images) 1,000 times and compute an overall error as the root mean square error (Stegun and Abramowitz, 1965):

$$RMSE = \sqrt{\frac{\sum_{i=1}^{1000} e_i^2}{1000}} \quad (3)$$

where e_i is the error brought about by the use of HAIR in the i -th iteration. By systematically changing the values of N as well as the maximal depth, d_0 , the trend of the RMSE values is then used to identify a robust final HAIR that can be applied to derive accurate road traffic metrics using new camera feeds.

We expect the RMSE to decrease and then converge when N and d_0 increase, a trend that can be used to determine the parameters to derive the final HAIR. The RMSE values for the 6 cameras under different parameter settings are shown in [Figure 7](#). It can be observed that the RMSE values tend to decrease and then stay at a low value when N and d_0 increase. Specifically, increasing the maximal depth (d_0) value while fixing the number of images (N) leads to a decrease in the RMSE. This trend suggests that further dividing the images can help discover additional (and small) areas where vehicles can be correctly detected and thus contribute to improving the coverage of the HAIR to include more correctly detected vehicles within the entire image extent. However, when the d_0 value is too high (larger than 4 in our case), the RMSE remains approximately unchanged in further subdivisions. This is because further subdividing the images will produce the sub-quadrants that are too small to cover new correctly detected vehicles in the images, which are unlikely to be considered for the HAIR. On the other hand, when the maximal depth (d_0) is fixed, increasing the number of images (N) to derive the HAIR contributes to the decrease in RMSE. The decrease diminishes when the N value reaches a certain level, showing a trend of convergence in the error of HAIR and suggesting it is not necessary to continuously increase the N value to reach a robust coverage of detected vehicles in the HAIR. There are two exceptions when d_0 is 1 for cameras [4] and [6], but based on the previous discussion about the effect of d_0 , all our experiments show d_0 needs to be higher than 1 to achieve the accuracy threshold.

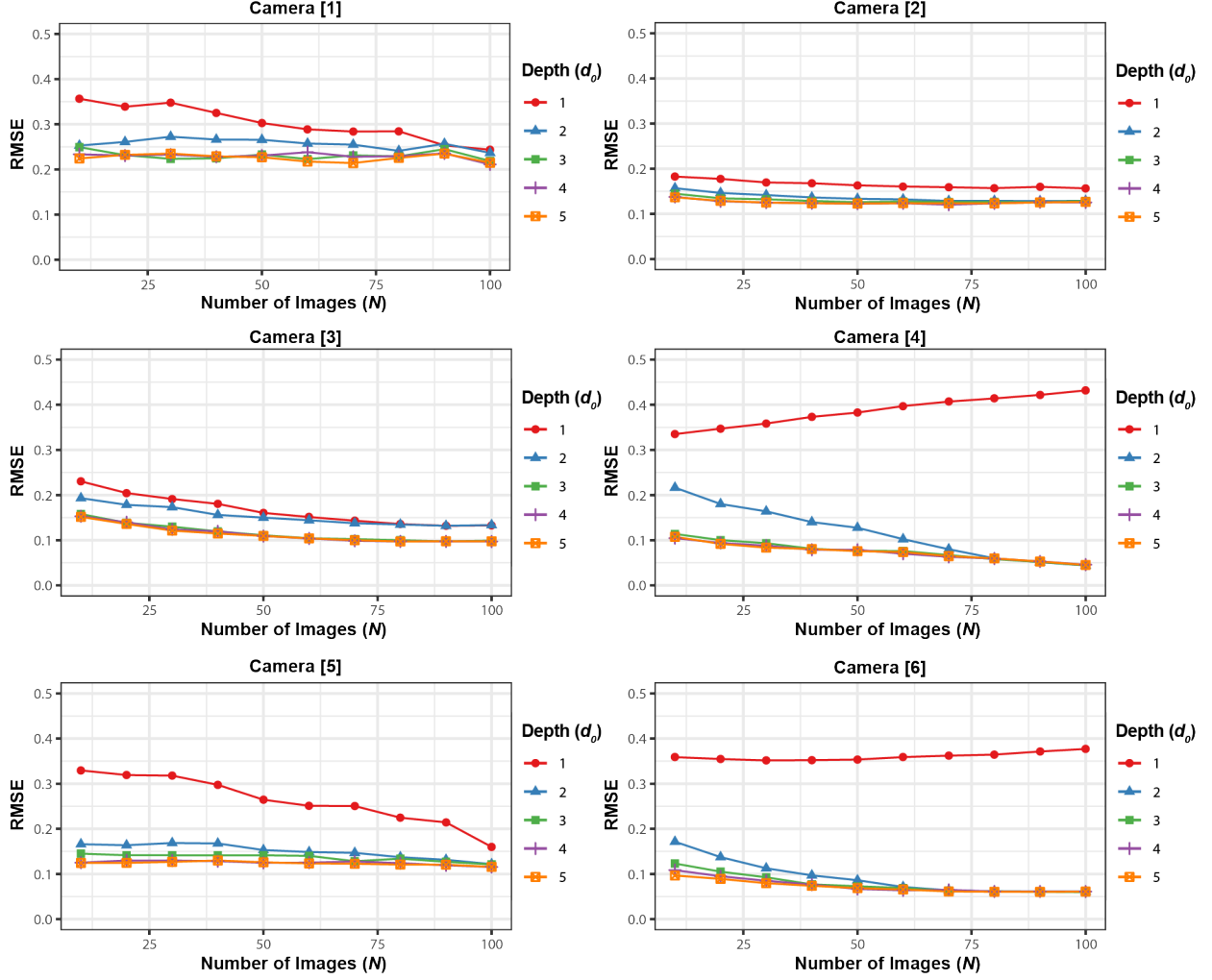


Figure 7. The average error of the HAIR (RMSE) at different numbers of images (N) and maximal depths (d_0) for the selected 6 cameras.

The N and d_0 values used to identify the final HAIR for each camera can be determined based on the RMSE trends (Figure 7). When the depth increases from i to j with the number of images being k ($1 \leq i < j \leq 5$ and $1 \leq k \leq N$, where 5 is the maximal depth as used in this study), we define the decrease in RMSE as Δ_{ijk} . The final maximum depth (d_0^*) is determined as the smallest i value that satisfies the condition of $\Delta_{ijk} \leq 0.01$, for all i, j , and k values. Here, the value of 0.01 is a threshold representing a decrease in RMSE without significant gain in accuracy. This yields the smallest depth where further increasing the depth will not bring up significant gains in accuracy. Once the d_0^* value is determined, we determine the final number of images (N^*) for a given camera to be the smallest k value that satisfies the condition of $\Delta_{d_0^*jk} \leq 0.001$, for all j and k values where $j > d_0^*$. The final N^* and d_0^* values for the 6 cameras are listed in Table 1. The small maximal depth values (3 or 4) in Table 1 suggest the efficiency of the algorithm as the running time is determined by the depths (Xiao, 2016).

Table 1. Final values for the number of images (N^*) and maximal depth (d_0^*) for the 6 cameras.

| Camera | N^* | d_0^* |
|--------|-------|---------|
| [1] | 40 | 4 |

| | | |
|-----|----|---|
| [2] | 20 | 3 |
| [3] | 50 | 3 |
| [4] | 50 | 3 |
| [5] | 30 | 4 |
| [6] | 40 | 3 |

We use 50 annotated images (where vehicles are identified and labeled) collected from the same 6 cameras but not used in the identification of the HAIR to evaluate the effectiveness of the HAIR. The detection accuracies for both the original image extent and the HAIR are presented in Table 2. A precision value here is the ratio between the number of correctly detected vehicles and all detected, and a recall is the ratio between the number of correctly detected vehicles and all labelled vehicles, in the image or the HAIR. The RAP values for the image and the HAIR are calculated as described in Section 3.1. The overall precision of the entire image extent is generally high for all the 6 cameras (0.972), but the overall recall values are relatively low (0.588 in average), especially for cameras [2] and [3]. This means that although more than 90 percent of the detections by the trained model are correct, a significant number of vehicles are still not identified, which also leads to the low RAP values (0.577 in average). The results clearly indicate that the overall recall and RAP inside the HAIR are significantly higher than that of the original image extent, with 48 and 41 percent increases, respectively. For cameras [2] and [3], the RAP within the HAIR reaches above 0.7, increases of 168 and 98 percent, respectively, over that within the image extent.

Table 2. Comparison of vehicle detection accuracy between the original image extent and the HAIR.

| Camera | Camera type | | Precision | | Recall | | RAP | |
|---------|-------------|------------|-----------|-------|--------|-------|-------|--------------|
| | Height | Resolution | Image | HAIR | Image | HAIR | Image | HAIR |
| [1] | Low | Low | 0.987 | 0.964 | 0.724 | 0.938 | 0.722 | 0.885 |
| [2] | High | Low | 0.993 | 1.000 | 0.209 | 0.717 | 0.271 | 0.727 |
| [3] | Low | Low | 0.992 | 0.981 | 0.367 | 0.755 | 0.362 | 0.717 |
| [4] | Low | Low | 0.992 | 0.982 | 0.772 | 0.969 | 0.722 | 0.895 |
| [5] | Low | High | 0.938 | 0.929 | 0.830 | 0.970 | 0.781 | 0.852 |
| [6] | High | High | 0.931 | 0.988 | 0.625 | 0.880 | 0.603 | 0.815 |
| Overall | | | 0.972 | 0.974 | 0.588 | 0.871 | 0.577 | 0.815 |

4.2 Traffic density estimation

To assess the effectiveness of the HAIR in traffic density estimation, we measure the predicted and observed traffic density values. For both extents of the entire image and the HAIR, the observed traffic density is calculated using number of the labeled vehicles and the road length with the extent, and the predicted traffic density is obtained using the detected vehicles only. Again, we use the 50 images mentioned above for each camera. For each image, the difference between the observed and predicted is estimated, and then the root mean square of the differences for the 50 images is calculated as the overall error. The root mean square errors for the entire image and the HAIR are presented in Table 3. It is clear that our proposed method using the HAIR can provide more accurate density estimates than those based on the original image extent, reducing overall error by 49 percent. For camera [3], the error is extremely high (9.939) if we directly use the vehicle count from the entire image. Our method significantly reduces the error to 3.539, a 64 percent improvement.

Table 3. Comparison of traffic density estimation between the original image extent and the HAIR.

| Camera | Camera type | | Image | Error |
|---------|-------------|------------|-------|--------------|
| | Height | Resolution | | |
| [1] | Low | Low | 3.858 | 1.760 |
| [2] | High | Low | 2.360 | 1.916 |
| [3] | Low | Low | 9.939 | 3.539 |
| [4] | Low | Low | 1.858 | 0.793 |
| [5] | Low | High | 2.210 | 2.102 |
| [6] | High | High | 0.733 | 0.603 |
| Overall | | | 3.493 | 1.785 |

5 Discussion and conclusions

This paper focuses on the areas within a camera view where vehicles can be correctly detected to enhance the road traffic estimates, and a quadtree based algorithm to identify such areas is presented and tested. Our experiments show that the vehicle detection accuracy within the HAIR is significantly higher than that in the entire image extent (Table 2), suggesting that the HAIR consistently exist in images with the same field of view. Our results also indicate the effectiveness of the proposed algorithm, where desired accuracy of vehicle detection can be achieved within the HAIR. The accurate vehicle counts within the HAIR can subsequently be used to improve the accuracy of road traffic estimates obtainable from traffic camera images (Table 3).

The application of this algorithm partly relies on manual spatial data operations such as georeferencing the images using ground control points. Applying this algorithm to a large number of cameras or real-time analysis on pan-tilt-zoom cameras will also demand an automatic procedure so that the road traffic metrics derived from the HAIR can be estimated without labor-intensive human input. Some recent progresses have potential addressing the issue of automation. High quality spatial data have become increasingly available as they are used to enable the recent surge of geodesign (Goodchild, 2010). Road data in in ArcGIS Urban¹, for example, have information about lanes and essential landmarks. 3D LiDAR data models are also used to automatically project 2D traffic images into the geographical space using deep neural networks (Cattaneo et al., 2020). Finally, studies on automated landmarks identification (Lin et al., 2019) make it possible to retrieve objects from traffic images that can be used for georeferencing. A fusion of these research outcomes is promising not only to improve the accuracy of automatic georeferencing but to enable more efficient traffic density estimation for real-time applications.

The proposed algorithm has the potential to contribute to a broader field in big data-driven transport and urban analytics. The past two decades have witnessed the emergence of big mobility data contributed by the proliferating location-aware devices such as various range sensors, GPS, and Wi-Fi (Leszczynski and Crampton, 2016), which have made it possible to address the data bottleneck for mobility research by providing large-scale human movement information in a convenient and affordable manner (Chen et al., 2016; Torre-Bastida et al., 2018). However, a significant portion of the available big mobility data sets such as mobile phone data and geotagged social media data are retrieved from private data providers where limited details of data production are released and only a few authorized users can gain access to the data (Xiao and Miller, 2021). The lack of transparency in data production and the barriers in data sharing have added difficulties in the assessment of data reliability and quality and have subsequently limited the use of such data (Haibe-Kains et al., 2020; Kwan, 2016). With the improvement in accuracy, the proposed algorithm can facilitate fully utilizing the new source of open geospatial big data, the publicly available traffic camera feeds, and contribute to the big data analytics for transportation

¹ <https://www.esri.com/arcgis-blog/products/urban/3d-gis/getting-started-with-arcgis-urban/>

and mobility research (Chen et al., 2016; Zhu et al., 2019). This algorithm can help extract accurate explicit movement information from open geospatial big data, and, more critically, provide reliable open mobility data products that have the potentials to overcome the barriers in transparency and accessibility imposed by other data sources.

References

- Black, J., 2018. *Urban transport planning: Theory and practice*. Routledge.
- Cao, L., Jiang, Q., Cheng, M., Wang, C., 2016. Robust vehicle detection by combining deep features with exemplar classification. *Neurocomputing* 215, 225–231. <https://doi.org/10.1016/j.neucom.2016.03.094>
- Cattaneo, D., Vaghi, M., Fontana, S., Ballardini, A.L., Sorrenti, D.G., 2020. Global visual localization in LiDAR-maps through shared 2D-3D embedding space. *Proc. - IEEE Int. Conf. Robot. Autom.* 4365–4371. <https://doi.org/10.1109/ICRA40945.2020.9196859>
- Chen, C., Ma, J., Susilo, Y., Liu, Y., Wang, M., 2016. The promises of big data and small data for travel behavior (aka human mobility) analysis. *Transp. Res. Part C Emerg. Technol.* 68, 285–299. <https://doi.org/10.1016/j.trc.2016.04.005>
- Chung, J., Sohn, K., 2018. Image-Based Learning to Measure Traffic Density Using a Deep Convolutional Neural Network. *IEEE Trans. Intell. Transp. Syst.* 19, 1670–1675. <https://doi.org/10.1109/TITS.2017.2732029>
- Conde Márquez, G.R., Escalante, H.J., Sucar, L.E., 2011. Simplified quadtree image segmentation for image annotation, in: *CEUR Workshop Proceedings*. pp. 24–34.
- Davis, S.C., Boundy, R.G., 2020. *Transportation Energy Data Book: Edition 38.2*. Oak Ridge National Laboratory, Oak Ridge, TN.
- de Palma, A., Lindsey, R., 2011. Traffic congestion pricing methodologies and technologies. *Transp. Res. Part C Emerg. Technol.* 19, 1377–1399. <https://doi.org/10.1016/j.trc.2011.02.010>
- Essen, H. van, Fiorello, D., El Beyrouy, K., Bieler, C., Wijngaarden, L., Lisanne van Schroten, A., Parolin, Riccardo Brambilla, M., Sutter, D., Maffii, S., Fermi, F., 2019. *Handbook on External Costs of Transport*. Publications Office of the European Union, Luxembourg. <https://doi.org/10.2832/27212>
- Everingham, M., Gool, L.J. Van, Williams, C., Winn, J.M., Zisserman, A., 2010. The Pascal Visual Object Classes (VOC) Challenge. *Int. J. Comput. Vis.* 88, 303–338.
- Fattal, A.K., Karg, M., Scharfenberger, C., Adamy, J., 2018. Distant vehicle detection: How well can region proposal networks cope with tiny objects at low resolution?, in: *Proceedings of the European Conference on Computer Vision (ECCV)*. pp. 289–304. https://doi.org/10.1007/978-3-030-11009-3_17
- Goodchild, M.F., 2010. Towards geodesign: Repurposing cartography and GIS? *Cartogr. Perspect.* 7–21. <https://doi.org/10.14714/cp66.93>
- Haibe-Kains, B., Adam, G.A., Hosny, A., Khodakarami, F., Waldron, L., Wang, B., McIntosh, C., Kundaje, A., Greene, C.S., Hoffman, M.M., Leek, J.T., Huber, W., Brazma, A., Pineau, J., Tibshirani, R., Hastie, T., Ioannidis, J.P.A., Quackenbush, J., Aerts, H.J.W.L., Shradha, T., Kusko, R., Sansone, S.A., Tong, W., Wolfinger, R.D., Mason, C., Jones, W., Dopazo, J., Furlanello, C., 2020. The importance of transparency and reproducibility in artificial intelligence research. *Nature* 586, E14–E16. <https://doi.org/10.1038/s41586-020-2766-y>
- Huang, J., Rathod, V., Sun, C., Zhu, M., Korattikara, A., Fathi, A., Fischer, I., Wojna, Z., Song, Y., Guadarrama, S., Murphy, K., 2017. Speed/accuracy trade-offs for modern convolutional object detectors, in: *Proceedings of the IEEE Conference on Computer Vision and Pattern Recognition (CVPR)*. pp. 7310–7319. <https://doi.org/10.1109/CVPR.2017.351>
- Huang, Y., Tian, Y., Liu, Z., Jin, X., Liu, Y., Zhao, S., Tian, D., 2020. A Traffic Density Estimation Model Based on Crowdsourcing Privacy Protection. *ACM Trans. Intell. Syst. Technol.* 11, 46. <https://doi.org/10.1145/3391707>
- James, G., Witten, D., Hastie, T., Tibshirani, R., 2013. *An Introduction to Statistical Learning*. Springer.
- Kim, S., Lewis, M.E., White, C.C., 2005. Optimal vehicle routing with real-time traffic information. *IEEE Trans. Intell. Transp. Syst.* 6, 178–188. <https://doi.org/10.1109/TITS.2005.848362>
- Kwan, M.-P., 2016. Algorithmic geographies: Big data, algorithmic uncertainty, and the production of geographic knowledge. *Ann. Am. Assoc. Geogr.* 106, 274–282. <https://doi.org/10.1080/00045608.2015.1117937>

- Leduc, G., 2008. Road Traffic Data: Collection Methods and Applications (No. JRC 47967), Working Papers on Energy, Transport and Climate Change.
- Leszczynski, A., Crampton, J., 2016. Introduction: Spatial Big Data and everyday life. *Big Data Soc.* 3, 205395171666136. <https://doi.org/10.1177/2053951716661366>
- Lin, T.Y., Goyal, P., Girshick, R., He, K., Dollar, P., 2020. Focal Loss for Dense Object Detection. *IEEE Trans. Pattern Anal. Mach. Intell.* 42, 318–327. <https://doi.org/10.1109/TPAMI.2018.2858826>
- Lin, Y., Cai, Y., Gong, Y., Kang, M., Li, L., 2019. Extracting urban landmarks from geographical datasets using a random forests classifier. *Int. J. Geogr. Inf. Sci.* 33, 2406–2423. <https://doi.org/10.1080/13658816.2019.1620238>
- McDermott, R., 2011. Internal and External Validity, in: Druckman, J.N., Greene, D.P., Kuklinski, J.H., Lupia, A. (Eds.), *Cambridge Handbook of Experimental Political Science*. Cambridge University Press, pp. 27–40. <https://doi.org/10.1017/CBO9780511921452.003>
- O'Mahony, N., Campbell, S., Carvalho, A., Harapanahalli, S., Hernandez, G.V., Krpalkova, L., Riordan, D., Walsh, J., 2020. Deep Learning vs. Traditional Computer Vision, in: Arai, K., Kapoor, S. (Eds.), *Advances in Intelligent Systems and Computing*. Springer, Cham, pp. 128–144. https://doi.org/10.1007/978-3-030-17795-9_10
- Olszewski, P., Xie, L., 2005. Modelling the effects of road pricing on traffic in Singapore. *Transp. Res. Part A Policy Pract.* 39, 755–772. <https://doi.org/10.1016/j.tra.2005.02.015>
- R. Pal, N., K. Pal, S., 1993. A Review on Image Co-segmentation. *Pattern Recognition* 26, 1277–1294. [https://doi.org/10.1016/0031-3203\(93\)90135-J](https://doi.org/10.1016/0031-3203(93)90135-J)
- Ren, S., He, K., Girshick, R., Sun, J., 2017. Faster R-CNN: Towards Real-Time Object Detection with Region Proposal Networks. *IEEE Trans. Pattern Anal. Mach. Intell.* 39, 1137–1149. <https://doi.org/10.1109/TPAMI.2016.2577031>
- Samet, H., 1984. The Quadtree and Related Hierarchical Data Structures. *ACM Comput. Surv.* 16, 187–260. <https://doi.org/10.1145/356924.356930>
- Shin, C.S., Lee, J., Lee, H., 2020. Infrastructure-less Vehicle Traffic Density Estimation via Distributed Packet Probing in V2V Network. *IEEE Trans. Veh. Technol.* <https://doi.org/10.1109/TVT.2020.3019783>
- Smith, E., 2017. *History of Intelligent Transportation Systems (ITS): Connected Vehicles and Smart Cities*.
- Snyder, C., Do, M.N., 2019. STREETS: A Novel Camera Network Dataset for Traffic Flow, in: Wallach, H., Larochelle, H., Beygelzimer, A., D'Alché-Buc, F., Fox, E., Garnett, R. (Eds.), *Advances in Neural Information Processing Systems 32 (NIPS 2019)*. Curran Associates, Inc., New York, US, pp. 10242–10253.
- Sookun, A., Boojhawon, R., Rughooputh, S.D.D.V., 2014. Assessing greenhouse gas and related air pollutant emissions from road traffic counts: A case study for Mauritius. *Transp. Res. Part D Transp. Environ.* 32, 35–47. <https://doi.org/10.1016/j.trd.2014.06.005>
- Spann, M., Wilson, R., 1985. A quad-tree approach to image segmentation which combines statistical and spatial information. *Pattern Recognit.* 18, 257–269. [https://doi.org/10.1016/0031-3203\(85\)90051-2](https://doi.org/10.1016/0031-3203(85)90051-2)
- Stegun, I., Abramowitz, M., 1965. *Handbook of Mathematical Functions: with Formulas, Graphs, and Mathematical Tables*. Dover Publications, Mineola, NY.
- Tan, M., Pang, R., Le, Q. V., 2020. EfficientDet: Scalable and Efficient Object Detection, in: *Proceedings of the IEEE/CVF Conference on Computer Vision and Pattern Recognition (CVPR)*. pp. 10781–10790.
- Torre-Bastida, A.I., Del Ser, J., Laña, I., Ilardia, M., Bilbao, M.N., Campos-Cordobés, S., 2018. Big Data for transportation and mobility: Recent advances, trends and challenges. *IET Intell. Transp. Syst.* 12, 742–755. <https://doi.org/10.1049/iet-its.2018.5188>
- TrafficLand, 2020. TrafficLand Launches New Live Traffic Video Mobile App [WWW Document]. URL http://newsroom.trafficland.com/press_releases/contents/000/000/077/original/Press_Release_-_TrafficLand_Mobile_App_4.23.pdf?1556039965
- Wang, C., Liao, H.M., 2020. YOLOv4: Optimal Speed and Accuracy of Object Detection.

- Wang, H., Yu, Y., Cai, Y., Chen, X., Chen, L., Liu, Q., 2019. A Comparative Study of State-of-the-Art Deep Learning Algorithms for Vehicle Detection. *IEEE Intell. Transp. Syst. Mag.* 11, 82–95. <https://doi.org/10.1109/MITS.2019.2903518>
- Wang, J., Huang, Y., Feng, Z., Member, S., Jiang, C., Member, S., Zhang, H., Member, S., Leung, V.C.M., 2018. Reliable Traffic Density Estimation in Vehicular Network. *IEEE Trans. Veh. Technol.* 67, 6424–6437. <https://doi.org/10.1109/TVT.2018.2803062>
- Xiao, N., 2016. *GIS Algorithms*. SAGE Publications Inc., Thousand Oaks, CA.
- Xiao, N., Miller, H.J., 2021. Cultivating Urban Big Data, in: Shi, W., Goodchild, M., Batty, M., Kwan, M.-P. (Eds.), *Urban Informatics*. Springer, Singapore, pp. 547–565. https://doi.org/10.1007/978-981-15-8983-6_31
- Xu, J., Hilker, N., Turchet, M., Al-Rijleh, M.K., Tu, R., Wang, A., Fallahshorshani, M., Evans, G., Hatzopoulou, M., 2018. Contrasting the direct use of data from traffic radars and video-cameras with traffic simulation in the estimation of road emissions and PM hotspot analysis. *Transp. Res. Part D Transp. Environ.* 62, 90–101. <https://doi.org/10.1016/j.trd.2018.02.010>
- Zhang, S., Benenson, R., Omran, M., Hosang, J., Schiele, B., 2016. How far are we from solving pedestrian detection?, in: *Proceedings of the IEEE Conference on Computer Vision and Pattern Recognition (CVPR)*. IEEE, pp. 1259–1267. <https://doi.org/10.1109/CVPR.2016.141>
- Zhang, Z., Zheng, J., Xu, H., Wang, X., 2019. Vehicle Detection and Tracking in Complex Traffic Circumstances with Roadside LiDAR. *Transp. Res. Rec.* 2673, 62–71. <https://doi.org/10.1177/0361198119844457>
- Zhao, J., Xu, H., Liu, H., Wu, J., Zheng, Y., Wu, D., 2019. Detection and tracking of pedestrians and vehicles using roadside LiDAR sensors. *Transp. Res. Part C Emerg. Technol.* 100, 68–87. <https://doi.org/10.1016/j.trc.2019.01.007>
- Zhu, L., Yu, F.R., Wang, Y., Ning, B., Tang, T., 2019. Big Data Analytics in Intelligent Transportation Systems: A Survey. *IEEE Trans. Intell. Transp. Syst.* 20, 383–398. <https://doi.org/10.1109/TITS.2018.2815678>

Appendix. Deep learning model for vehicle detection.

Two data sets are created using the camera feeds in Central Ohio for the purposes of vehicle detection model training and evaluation. The first data set, referred to as *Odot1*, contains 1,392 images from the 249 cameras in Central Ohio, which is used to train the deep learning models for vehicle detection. These cameras cover different locations, camera conditions, and traffic states in the area and capture sufficient traffic scenes for model training. Images in this data set are collected during daytime hours (8am to 8pm) in August 2019 and are processed through an annotation process where bounding boxes of the vehicles are manually identified. Vehicles that are too small to visually identify ($< 2 \times 2$ pixels) are not labeled in this process.

The second data set employed in this study, named *Odot2*, is used to evaluate the trained vehicle detection models and to determine the best trained model for the use in subsequent steps of traffic density estimation. This data set consists of 465 traffic camera images in Central Ohio, which are also retrieved in August 2019. These images generally represent the new images that one may encounter within the study area and are used to evaluate how the trained vehicle detection models perform on new traffic images retrieved in the study area.

The deep learning literature generally suggests the use of a large and diverse training data set to improve detection accuracy (Halevy et al., 2009). For this reason, in addition to the images from the ODOT cameras, we enrich our training data set (*Odot1*) using the annotated images with labeled vehicles (i.e., vehicles that are manually identified and labeled) from two additional sources, STREETS (Snyder and Do, 2019) and WebCamT (Zhang et al., 2017), which contain 2,950 and 59,207 traffic camera images in the United States, respectively. Together with *Odot1*, the three data sets are combined in different ways for the training of the vehicle detection models.

EfficientDet (Tan et al., 2020a) is a family of 8 object detection models (EfficientDet-d0 through d7) which share the same architecture. EfficientDet-d0 is the baseline model, and each of the next model has a larger size measured by its depth (number of layers), width (size of layers), and input image resolution. A large model size generally means high detection accuracy and high computational intensity. In this study, we examine all these models except EfficientDet-d7, because scaling up from d6 to d7 significantly increases the costs of system memory and training time but has little improvement in the detection accuracy (Tan et al., 2020a).

Figure S1 presents the training and evaluation of EfficientDet for vehicle detection. We first combine data sets *Odot1*, STREET, and WebCamT in four different ways (labeled as D1 through D4 in the left column of Figure S1). Each of these combinations is used to train each of the 7 models of EfficientDet (center column in Figure S1). All trained models are evaluated on data set *Odot2* using the average precision (AP) metric (Everingham et al., 2010), and the goal is to select the trained model with the highest accuracy (right column in Figure S1). We implement the EfficientDet models in TensorFlow 2.3 (<https://www.tensorflow.org/>) using the source code released by Tan et al. (2020b). The experiments are conducted using NVIDIA Tesla P100 and V100 GPUs.

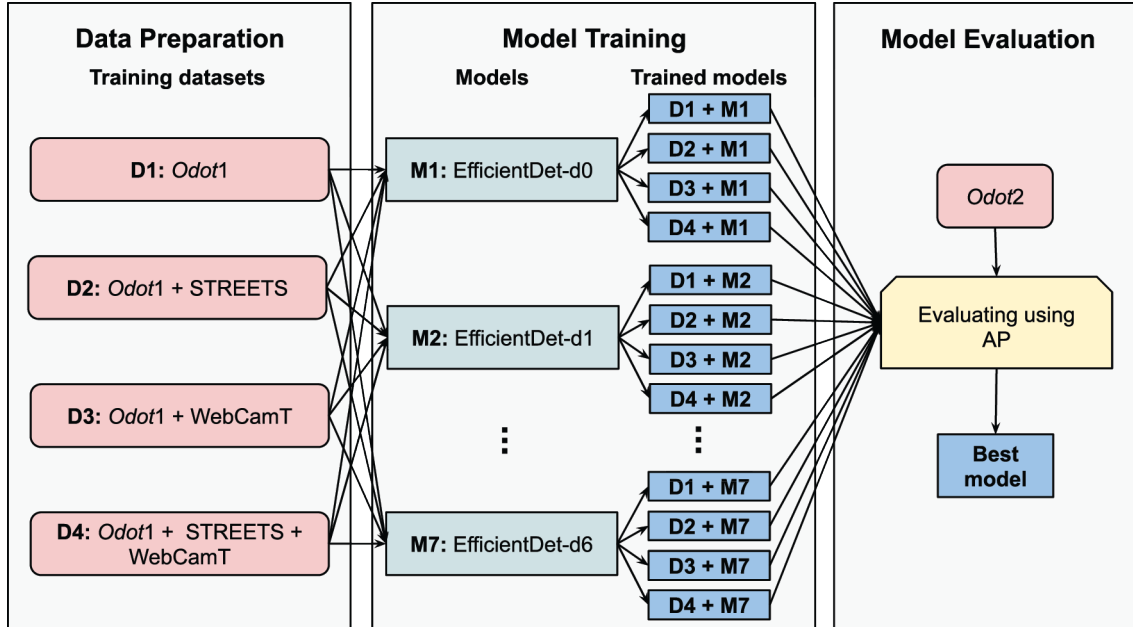


Figure S1. Flowchart of model training and evaluation for vehicle detection. AP: average precision.

The results of model evaluation are presented in [Table S1](#). As the models scale up from d0 to d5, the detection accuracy of EfficientDet increases, where the AP of EfficientDet-d5 almost doubles that of EfficientDet-d0 across all training data sets. Scaling the model up from d5 to d6, however, does not contribute to further gain in AP values for our specific cases. The two additional data sources have different impacts on accuracy as well. Adding STREETS data alone consistently improves approximately 10 percent for all the model settings. The use of WebCamT with *Odot1*, however, does not increase the model accuracy except for model d0 due to the significant difference in traffic scenes between the two sources. This also explains why the combination of all three data sets is outperformed by *Odot1*+STREETS. This result is consistent with previous studies found in the literature where prediction accuracy will eventually saturate and may even decrease with additional data, because the data amount and diversity have exceeded the complexity of the model (Zhu et al., 2016). We choose the detector with the highest accuracy, EfficientDet-d5 trained by *Odot1*+STREETS, for traffic density analysis in this study.

Table S1. Accuracy of the trained vehicle detection models measured by the AP. Evaluations are conducted using data set *Odot2*.

| Model | D1: <i>Odot1</i> | D2: <i>Odot1</i> + STREETS | D3: <i>Odot1</i> + WebCamT | D4: <i>Odot1</i> + STREETS + WebCamT |
|-----------------|------------------|----------------------------|----------------------------|--------------------------------------|
| EfficientDet-d0 | 0.142 | 0.160 | 0.150 | 0.153 |
| EfficientDet-d1 | 0.217 | 0.232 | 0.206 | 0.204 |
| EfficientDet-d2 | 0.255 | 0.277 | 0.204 | 0.258 |
| EfficientDet-d3 | 0.279 | 0.313 | 0.240 | 0.274 |
| EfficientDet-d4 | 0.292 | 0.327 | 0.277 | 0.295 |
| EfficientDet-d5 | 0.338 | 0.354 | 0.293 | 0.333 |
| EfficientDet-d6 | 0.337 | 0.353 | 0.273 | 0.322 |

It should be noted that even the best model evaluated here can only reach an AP of 0.354, meaning that the detection precision decreases rapidly when increasing the vehicle instances in the evaluation. With all the detected instances from *Odot2*, the precision of this model can reach 0.954, but the recall is 0.357, which indicates that many vehicles are still missed by the detection model. These results are consistent with Wang et al. (2019), which indicates that a large number of small objects (distant vehicles) are difficult to detect by existing models and tend to result in low detection accuracy overall. The model as such, when used for traffic density estimation, clearly will lead to significant error and therefore it is imperative to obtain accurate vehicle count and density estimation.

References

- Everingham, M., Gool, L.J. Van, Williams, C., Winn, J.M., Zisserman, A., 2010. The Pascal Visual Object Classes (VOC) Challenge. *Int. J. Comput. Vis.* 88, 303–338.
- Halevy, A., Norvig, P., Pereira, F., 2009. The reasonable effectiveness of data. *IEEE Intell. Syst.* 24, 8–12.
- Snyder, C., Do, M.N., 2019. STREETS: A Novel Camera Network Dataset for Traffic Flow, in: Wallach, H., Larochelle, H., Beygelzimer, A., D’Alché-Buc, F., Fox, E., Garnett, R. (Eds.), *Advances in Neural Information Processing Systems 32 (NIPS 2019)*. Curran Associates, Inc., New York, US, pp. 10242–10253.
- Tan, M., Pang, R., Le, Q. V., 2020a. EfficientDet: Scalable and Efficient Object Detection, in: *Proceedings of the IEEE/CVF Conference on Computer Vision and Pattern Recognition (CVPR)*. pp. 10781–10790.
- Tan, M., Pang, R., Le, Q. V., 2020b. EfficientDet [WWW Document]. URL <https://github.com/google/automl/tree/master/efficientdet>
- Wang, H., Yu, Y., Cai, Y., Chen, X., Chen, L., Liu, Q., 2019. A Comparative Study of State-of-the-Art Deep Learning Algorithms for Vehicle Detection. *IEEE Intell. Transp. Syst. Mag.* 11, 82–95. <https://doi.org/10.1109/MITS.2019.2903518>
- Zhang, S., Wu, G., Costeira, J.P., Moura, J.M.F., 2017. Understanding Traffic Density from Large-Scale Web Camera Data, in: *Proceedings of the IEEE Conference on Computer Vision and Pattern Recognition (CVPR)*. Honolulu, HI, USA, pp. 4264–4273. <https://doi.org/10.1109/CVPR.2017.454>
- Zhu, X., Vondrick, C., Fowlkes, C.C., Ramanan, D., 2016. Do We Need More Training Data? *Int. J. Comput. Vis.* 119, 76–92. <https://doi.org/10.1007/s11263-015-0812-2>